Cocrystallization improves the tabletability of ligustrazine despite a reduction in plasticity

Gerrit Vreeman, a,1 Danyingzi Guan, b,1 Yuncheng Cai,c Qun Zhou, b,\* and Changquan Calvin Suna,\*

<sup>a</sup> Pharmaceutical Materials Science and Engineering Laboratory, Department of Pharmaceutics,

College of Pharmacy, University of Minnesota, Minneapolis, MN 55455, United States

<sup>b</sup> Hubei Key Laboratory of Natural Medicinal Chemistry and Resource Evaluation, Tongji School

of Pharmacy, Huazhong University of Science and Technology, Wuhan 430030, China

<sup>c</sup> Analytical & Testing center, Huazhong University of Science and Technology, Wuhan 430074,

China

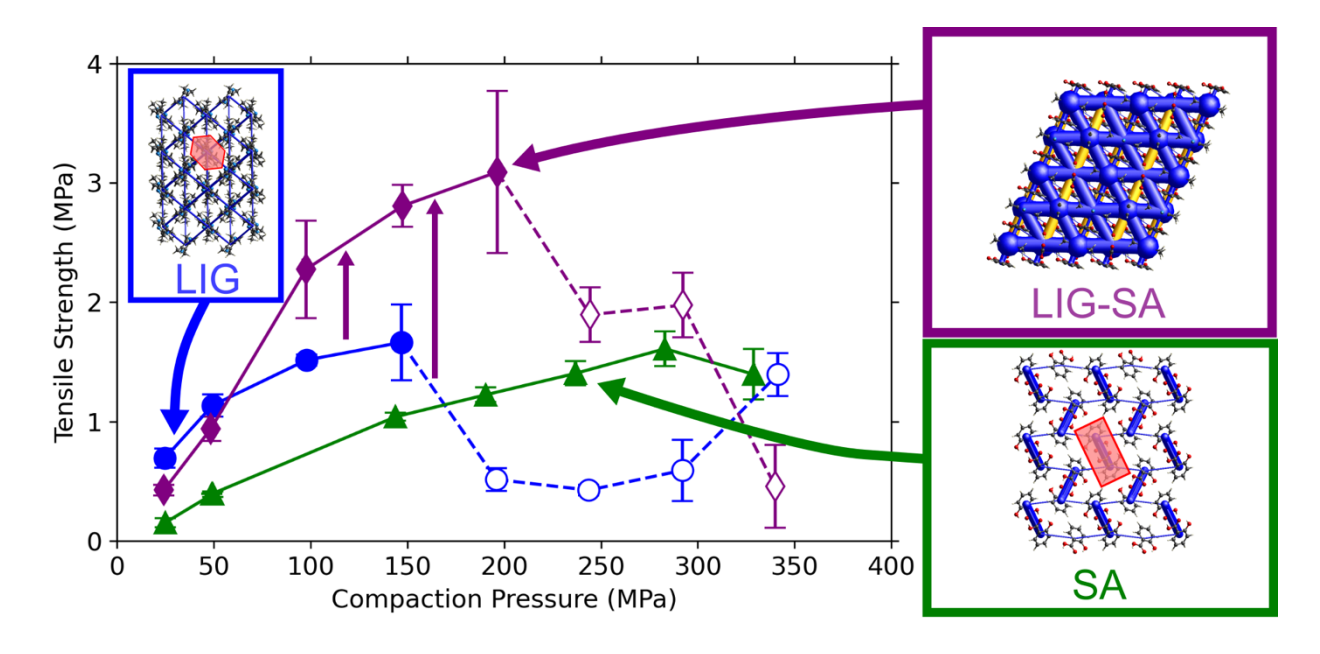
<sup>1</sup> These authors contributed equally to this work.

\*Corresponding authors:

Changquan Calvin Sun, Tel.: 612-624-3722; fax: 612-626-2125; email: sunx0053@umn.edu.

Qun Zhou, Tel.: 86-27-13807194659; fax: 86-27-83692793, email: zqtcm@hust.edu.cn

# **Graphical Abstract**



## Abstract

Cocrystallization is an effective method for altering the tableting performance of crystals by modifying their mechanical properties. In this study, cocrystals of ligustrazine (LIG) with malonic acid (MA) and salicylic acid (SA) were investigated to better understand how modifying crystal structure can affect tableting properties. LIG suffered from overcompression at high pressures despite its high plasticity. Both LIG-MA and LIG-SA displayed lower plasticity than LIG, which was confirmed by both an in-die Heckel and energy framework analyses. The LIG-MA cocrystal displayed slightly worse tabletability than LIG, as expected from its lower plasticity. However, LIG-SA surprisingly showed improved tabletability despite its lower plasticity. This was explained by the higher bonding strength of LIG-SA compared with LIG. This work not only provided new examples of tabletability modulation through crystal engineering but also highlighted the risk of failed tabletability predictions based on plasticity alone. Instead, more reliable tabletability predictions of different crystal forms must consider the bonding area – bonding strength interplay.

**Keywords:** ligustrazine; cocrystal; salt; plasticity; tabletability; structure-property

- **Abbreviations:**
- 19 LIG: ligustrazine; MA: malonic acid; SA: salicylic acid; API: active pharmaceutical ingredient;
- 20 SCXRD: single-crystal X-ray diffractometry; PXRD: powder X-ray diffractometry

#### 1 Introduction

21

22

23

24

25

26

27

28

29

30

31

32

33

34

35

36

37

38

39

40

41

42

43

Ligustrazine (LIG, Figure 1a) is the main active compound of a Chinese traditional medicine, Ligusticum chuanxiong. It has been clinically used for treating cerebral thrombosis, coronary heart disease, and angina pectoris due to its effects of vasodilation, platelet aggregation inhibition, thrombosis prevention, and cerebral ischemia improvement (Gao et al., 2015; Kao et al., 2006; Li et al., 2017; Liao et al., 2004; Lin et al., 2015; Ren et al., 2012). Both injections and oral solid dosage forms (tablets or capsules) of LIG are available. Injection administration of LIG has been applied to treat cardiovascular diseases in China, but the safety problems on the herbal injection have usually been a serious concern. Thus, oral delivery is preferable for chronic diseases and convenient for patients to use (Guo et al., 2016; Zhao et al., 2016). In contrast, oral administration of LIG offers higher patient compliance due to its convenience and pain-free nature. Oral administration also eliminates the risk of cross infection through needles, making it more preferred for administering LIG. These advantages are particularly important for treating chronic diseases using LIG (Cao et al., 2016). However, commercial hydrochloride salt form of LIG (LIG-HCl) are challenging for tablet development because of their high sublimation tendency under ambient conditions and poor tabletability (Hu et al., 2020). Thus, new crystal forms of LIG exhibiting improved physical stability and compaction properties would be useful for developing high quality tablets of LIG. Having previously addressed the high sublimation tendency issues of solid LIG through salt formation with acesulfame (Hu et al., 2020), we now turn our attention to enhancing its tabletability using crystal engineering. Several examples have shown the effectiveness of cocrystallization in modifying mechanical properties and, hence, tableting performance of active

pharmaceutical ingredients (API) (Karki et al., 2009; Sun, 2009; Wang et al., 2020). In pursuit of

enhancing LIG's tabletability, we synthesized two new cocrystals: one with malonic acid (MA, Figure 1b) and another with salicylic acid (SA, Figure 1c). Crystals with higher plasticity are typically assumed to exhibit superior tabletability by promoting a larger bonding area (BA) between neighboring particles during compression (Chow et al., 2012; Liu et al., 2018; Sun and Hou, 2008). However, we observed that the LIG-SA salt cocrystal is an exception where a less plastic cocrystal exhibits better tabletability because of a higher bonding strength (BS). Although this scenario is expected from the BA-BS interplay model (Osei-Yeboah et al., 2016; Sun, 2011), no examples have been reported in the literature. This work emphasizes the importance of applying a holistic, scientific understanding in guiding effective crystal engineering to overcome tabletability challenges of APIs. By including candidate crystal forms with lower plasticity, an expanded crystal engineering design space is introduced, offering new avenues for improving tabletability.

**Figure 1.** Molecular structures of (a) ligustrazine (LIG), (b) malonic acid (MA), and (c) salicylic acid (SA).

# 2 Experimental Section

#### 2.1 Materials

59

60

64

71

79

- Malonic acid (MA, BeanTown Chemical, Hudson, NH) and salicylic acid (SA, Sigma-
- 62 Aldrich, St. Louis, MO) were used as received. Ligustrazine hydrochloride (LIG-HCl, Yanjing
- 63 Pharmaceutical Industry, Beijing, China) was used to prepare anhydrous LIG.

## 2.2 LIG powder preparation

- 65 LIG powder was prepared by dissolving about 30 g of LIG-HCl in a small amount of water
- to form a concentrated solution. The solution was neutralized with excess sodium hydroxide and
- 67 LIG was extracted from the solution using ethyl acetate aided by a separatory funnel. The LIG-
- 68 containing ethyl acetate layer was dried using a rotary evaporator to obtain solid LIG, which was
- 69 lightly milled in a mortar by a pestle. The LIG powder was further dried in a desiccated chamber
- overnight. Phase purity of the LIG powder was verified by PXRD prior to tableting (Figure S1).

# 2.3 Cocrystal powder preparation

- 72 LIG-MA powder was prepared by slurrying a 1:1 stoichiometric molar mixture of LIG and
- 73 MA (totaling about 10 g) at 55 °C in an excess ethanol-acetone 6:1 volume ratio (v/v) mixture.
- 74 LIG-SA powder was prepared by slurrying a 1:2 stoichiometric molar mixture of LIG and SA
- 75 totaling about 15 g at a controlled temperature of ~55 °C in an excess ethanol-acetone 6:1 v/v
- 76 mixture. The powders were isolated using vacuum filtration, lightly milled using a mortar and
- pestle, then left to dry overnight at ambient conditions. Phase purity was assessed by PXRD before
- 78 tableting (Figure S1).

## 2.4 Single-crystal X-ray diffractometry (SCXRD)

- 80 LIG-SA single crystals were prepared by mixing 0.005 mol LIG and 0.01 mol SA in a
- 20 mL glass vial. LIG-MA single crystals were prepared by mixing 0.005 mol LIG and 0.005 mol

MA in a 20 mL glass vial. An ethanol-acetone 6:1 (v/v) solvent mixture was gradually added to the vials while heating at 55 °C in a water bath. Supersaturated solutions were left to cool at room temperature undisturbed for several days. Crystals were examined under an optical microscope and suitable crystals were selected for structure solution by single-crystal X-ray diffractometry (SCXRD) to gain insights into the molecular arrangement and intermolecular interactions in LIG-SA and LIG-MA. A Rigaku XtaLAB PRO MM007HF (rotating anode) diffractometer, equipped with a PILATUS200K/R CCD plate detector was used to collect diffraction data at 100 K, using Cu K $\alpha$  radiation (multilayer monochromator,  $\lambda = 1.54184$  Å), with the  $\omega$ -scans method. Crystal structures were solved using SHELXT and refined using SHELXL in the Olex2 interface (Dolomanov et al., 2009; Sheldrick, 2015a, 2015b).

# 2.5 Powder X-ray diffractometry (PXRD)

Powder phase purity was evaluated using a powder X-ray diffractometer (X'Pert PRO, PANalytical Inc., West Borough, MA) equipped with a reflection-transmission spinner set at a revolution time of 16 s and a copper X-ray source (45 kV and 40 mA) to provide  $K_{\alpha}$  radiation (1.5406 Å) over a 5° to 35° 20 range using a 0.017° step size and a dwell time of 0.514 s. The incident beam path was equipped with a 0.04 rad soller slit, a 10 mm fixed incident beam mask, a fixed 1/16° divergence slit, and a fixed 1/8° anti-scatter slit. The diffracted beam path was equipped with a beta nickel filter, a 0.04 rad soller slit, and a 5.5 mm anti-scatter slit (X'Celerator). Mercury (V. 2023.2.0, CCDC, Cambridge, UK) was used to calculate PXRD patterns from the crystal structures with step size of 0.02°.

## 2.6 Thermogravimetric analysis

Thermogravimetric analysis (TGA) was performed to assess cocrystal stability using a thermogravimetric analyzer (Q50, TA Instruments, New Castle, DE) with an N<sub>2</sub> purge at a heating

rate of 10 °C/min from room temperature to 200 °C (Figure S2). Stability was further examined by measuring the weight loss under isothermal conditions at 40 °C and 80 °C after 1 hour.

## 2.7 Tableting

Tablets were prepared on a compaction simulator (Styl'One Evolution; MedelPharm, Beynost, France) with pressures ranging 10 MPa to 350 MPa. A symmetrical, force-controlled, single-compression cycle (composed of a 1 s rise and a 1 s fall without holding at the maximum force, followed by a 3 s relaxation and a 2 s ejection step) was used. Round, flat-faced tooling (8 mm in diameter) was used to compress the powder (approximately 200 mg). External lubrication was employed using magnesium stearate spray (Styl'One Mist, MedelPharm, Beynost, France, 0.3 mg/puff, 3-4 puffs were used to fully coat the die and punches). External lubrication was not used for LIG-MA and SA due to severe punch sticking (Xiang and Sun, 2023).

# 2.8 True density and tablet porosity

The out-of-die tablet densities ( $\rho$ ) were calculated from tablet dimensions, and tablet mass (w), using equation (1). Tablet diameter, D, and thickness, h, were measured with a caliper with an attachment to avoid the effect of tablet flashing on tablet thickness, h, value (Paul et al., 2017). Tablet weight was measured using an analytical balance.

$$\rho = \frac{w}{\pi \left(\frac{D}{2}\right)^2 h} \tag{1}$$

The true density  $(\rho_t)$  of SA, MA, LIG-SA, and LIG-MA powders was determined using helium pycnometry (Quantachrome Instruments, Ultrapycnometer 1000e, Boynton Beach, Florida) under ambient conditions. An accurately weighed sample (1-2 g) was placed into the sample cell. The experiment was repeated, and the data collection was concluded when the

variation between five consecutive measurements fell below 0.005 %. The mean of the last five measurements was taken as the  $\rho_t$ .

The  $\rho_t$  of pure LIG was determined using the Sun method, where out-of-die  $P-\rho$  data was fitted with equation (2) (Sun, 2004), where  $\varepsilon_c$  is a fitted critical porosity parameter (Figure S4) (Kuentz and Leuenberger, 1999).

131 
$$P = \frac{1}{C} \left[ (1 - \varepsilon_c) - \frac{\rho}{\rho_t} - \varepsilon_c \ln \left( \frac{1 - \frac{\rho}{\rho_t}}{\varepsilon_c} \right) \right]$$
 (2)

This was done to avoid gross errors in  $\rho_t$  due to sublimation during the helium pycnometry measurement (Chang et al., 2019). The values of  $\rho_t$  for all materials are tabulated in Table 1. Tablet porosity ( $\varepsilon$ ) was subsequently calculated using equation (3).

$$\varepsilon = 1 - \frac{\rho}{\rho_t} \tag{3}$$

# **2.9 Tablet tensile strength**

Tablet tensile strength ( $\sigma$ ) was calculated using equation (4), where F is breaking force (Fell and Newton, 1970). The cylindrical tablets were broken diametrically using a texture analyzer (TA-XT2i, Texture Technology Corps, NY) equipped with a 30 kg load cell with a trigger force of 5 g at a test speed of 0.01 mm/s.

$$\sigma = \frac{2F}{\pi Dh} \tag{4}$$

The  $\sigma$  at zero porosity ( $\sigma_0$ ) was obtained by regression of  $\sigma$ - $\varepsilon$  data to equation (5) where b is an empirical decay constant, as proposed by Ryshkewitch and Duckworth (Ryshkewitch, 1953).

$$\sigma = \sigma_0 e^{-b\varepsilon} \tag{5}$$

# 2.10 Plasticity assessment

Plasticity was assessed using the in-die Heckel analysis (Heckel, 1961a, 1961b; Vreeman and Sun, 2021). In-die  $\varepsilon$  data was calculated from dynamically measured tablet thickness during compaction, die diameter, and tablet mass determined after ejection. The in-die mean yield pressure  $(P_{y,i})$  was obtained from a linear regression of the linear portion of the Heckel plot  $(-\ln(\varepsilon) \text{ versus } P)$  according to equation (6), where A is a constant (Figure S5).

$$-\ln(\varepsilon) = \frac{1}{P_{y,i}}P + A \tag{6}$$

# 2.11 Energy framework

The intermolecular interaction energy was calculated with the B3LYP-D2/6-31G(d,p) molecular wavefunction (CrystalExplorer V.21.3) for each molecule using NWChem as a wavefunction source (Aprà et al., 2020; Mackenzie et al., 2017; Spackman et al., 2021). The total intermolecular interaction energy is the sum of the electrostatic, polarization, dispersion, and exchange-repulsion components for a given molecule with respective scale factors of 1.057, 0.740, 0.871, and 0.618. Interaction energies of a selected molecule were calculated for all molecules with any atom within 3.8 Å. For LIG-SA, the lower occupancy hydroxyl group on the disordered SA molecule was deleted using Mercury's (V2023.2.0, CCDC, Cambridge, UK) edit structure feature before the calculation. Unless otherwise specified, the energy framework cylinder thickness was set to 100 and the interaction energies below 10 kJ/mol were omitted for clarity.

#### Results and Discussion

## 3.1 Single crystal structure of the LIG cocrystals

The LIG-MA cocrystal (Figure 2a, CCDC deposition number 2330797) crystallizes in the monoclinic  $P2_1/c$  space group with unit cell parameters a = 9.4854 Å, b = 18.1925 Å, c = 18.1925 Å

7.3424 Å, and  $\beta = 108.42^{\circ}$ . The asymmetric unit contains an OH···N hydrogen bond between the hydroxyl group of a carboxyl group on MA and a nitrogen on LIG (Figure 2a).

is expected (Childs et al., 2007).

The LIG-SA cocrystal (Figure 2b, CCDC deposition number 2330798) is a rare example of salt cocrystal that crystallizes in the monoclinic Cc space group with unit cell parameters of a=11.9433 Å, b=13.4844 Å, c=13.3089 Å, and  $\beta=112.28^{\circ}$ . A salt between one of the SA molecules and LIG is formed via a proton transfer from the carboxyl group of SA to the nitrogen on the adjacent LIG. The hydroxyl group on the SA<sup>-</sup> anion is disordered over two positions with an occupancy of 0.715 and 0.285. A neutral SA molecule forms a hydrogen bond with the carbonyl oxygen on the SA<sup>-</sup> anion. The molecular planes of the LIG<sup>+</sup> cation and neutral SA molecule are parallel to each other, and both are perpendicular to the molecular plane of the SA<sup>-</sup> anion. This neutral SA molecule forms an OH···O hydrogen bond with the carboxylate group on the SA<sup>-</sup> anion. Based on the reported p $K_a$  values (3.6 for LIG (Zheng et al., 2018), 2.98 for SA (O'Neil, 2006), and 2.85 for MA (Kortüm et al., 1960), the  $\Delta pK_a$  value is 0.62 for the LIG-SA system and 0.75 for the LIG-MA system. Since both  $\Delta pK_a$  values are between 0 and 3, either a salt or cocrystal

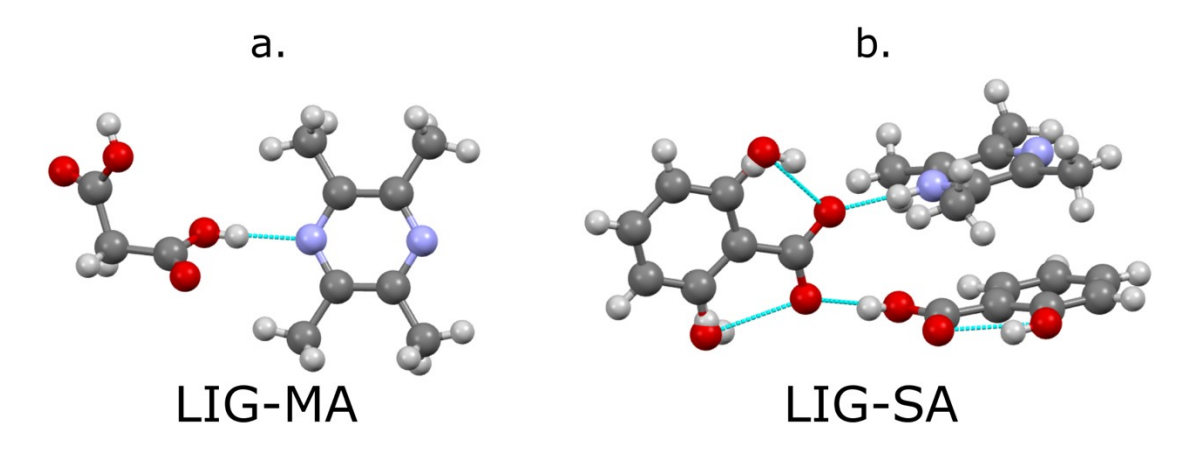


**Figure 2.** An asymmetric unit in (a) LIG-MA and (b) LIG-SA.

# 3.2 Tabletability

Both LIG-MA and LIG-SA powders were phase-pure based on PXRD data (Figure S1). They also had a higher physical stability against sublimation compared to the commercial LIG-HCl (Figure S2) or LIG freebase (Figure S3). The tablet tensile strength of LIG rises to about 1.6 MPa as compaction pressure increases to 150 MPa (Figure 3). Increasing the pressure further results in a decrease in tensile strength, i.e., overcompression took place (Figure 3). The overcompression is not accompanied by observable external defects and compaction did not lead to a detectable phase change. Thus, internal structural defects resulting from entrapped air may be responsible (Paul and Sun, 2017; Vreeman and Sun, 2022).

Compared to LIG, the tabletability of the LIG-MA cocrystal was much worse at pressures <150 MPa, but better at pressures >150 MPa (Figure 3a). Compared to MA, the LIG-MA cocrystal tabletability is only slightly improved at all compaction pressures. This result shows that effects of cocrystallization on tabletability may be pressure dependent.

The tabletability of the LIG-SA cocrystal is lower than LIG at compaction pressures ≤50 MPa, but it surpasses LIG between pressures of 100 MPa and 300 MPa. However, the tabletability of LIG-SA becomes lower than LIG at 340 MPa due to a sharp decrease above

280 MPa (Figure 3b). Since commercial tablets are usually compressed in the pressure range of 150 MPa to 300 MPa, the tabletability of LIG-SA is significantly improved over LIG within this practical pressure range. In fact, tablets with >2 MPa tensile strength could be attained by LIG-SA in the pressure range of 100 MPa to 240 MPa, indicating its adequate tabletability (Sun et al., 2009). In contrast, LIG cannot be compressed into a tablet with a tensile strength of 2 MPa over the entire pressure range investigated. Therefore, in terms of tabletability, LIG-SA is a good alternative crystal form to LIG for use in tablet formulation. Compared to SA, the tabletability of LIG-SA is significantly higher until the compaction pressure exceeds 300 MPa (Figure 3b).

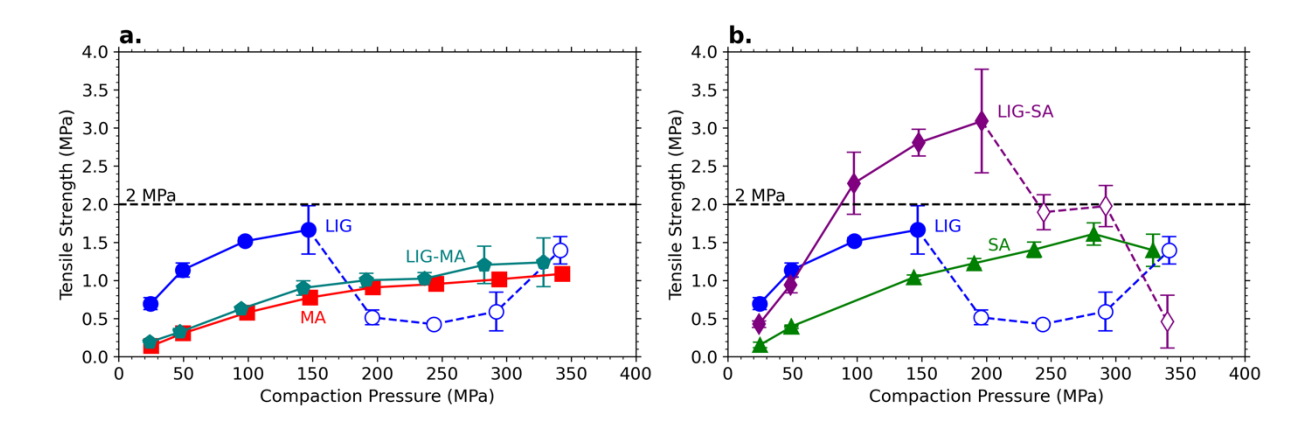


**Figure 3.** (a) Tabletability for LIG (blue circles), MA (red squared), and LIG-MA (teal pentagons) and (b) tabletability for LIG, SA (green triangles), and LIG-SA (purple diamonds). Open symbols indicate overcompressed tablets.

### 3.3 Component plasticity

An improved tabletability of LIG-SA compared with LIG (Figure 3b) may be explained by considering the relative contributions of BA and BS to tensile strength, in alignment with the BA-BA interplay model. Considering BA, the plasticity of each component was compared using the in-die mean yield pressure  $(P_{y,i})$ , where a lower  $P_{y,i}$  indicates a higher plasticity. Interestingly, LIG-SA  $(P_{y,i} = 90.1 \text{ MPa})$  is significantly less plastic than LIG  $(P_{y,i} = 52.5 \text{ MPa})$ , indicating that,

despite its improved tabletability, LIG-SA has a lower BA. To further corroborate the lower plasticity of LIG-SA compared to LIG, a crystal energy framework analysis was performed. The analysis revealed that the energy framework of LIG appears relatively isotropic with similar interaction energies present in orthogonal directions, and there is no indication of a clear facial slip system (Figure 4). However, a close inspection of the crystal structure of LIG revealed a columnar structure of LIG molecules running along the  $[0\bar{1}1]/[01\bar{1}]$  and  $[011]/[0\bar{1}\bar{1}]$  directions, allowing for facile slip and, therefore, reasonable plasticity (Chattoraj et al., 2010; Chow et al., 2012). Additionally, despite being relatively isotropic, LIG has significantly lower interaction energies compared to LIG-SA. Thus, slip may be easily activated during compression given the quasihydrostatic nature of in-die compression and random contacts between crystals in the powder bed (Vreeman et al., 2021), leading to a higher plasticity of LIG compared to LIG-SA. SA also has column-like structures, but unlike LIG, slip is only available in the  $[001]/[00\overline{1}]$  direction (Figure 4), which explains its slightly lower plasticity ( $P_{v,i} = 68.3 \text{ MPa}$ ) compared to LIG. In contrast, the energy framework of LIG-SA, although also relatively isotropic, is significantly stronger (Figure 4). This is consistent with presence of ionic interaction between LIG<sup>+</sup> and SA<sup>-</sup> ions and the hydrogen bonds of the salt pair with the neutral SA molecule. For clarity, the energy tube size of LIG-SA was set to half that of the other structures. The presence of repulsive energies (yellow tubes) in the LIG-SA energy framework is due to the repulsion between similarly charged molecules. Thus, the experimentally observed lower plasticity of LIG-SA compared to LIG and SA is supported by the analysis of their crystal structures and strength of their intermolecular interactions.

219

220

221

222

223

224

225

226

227

228

229

230

231

232

233

234

235

236

237

238

239

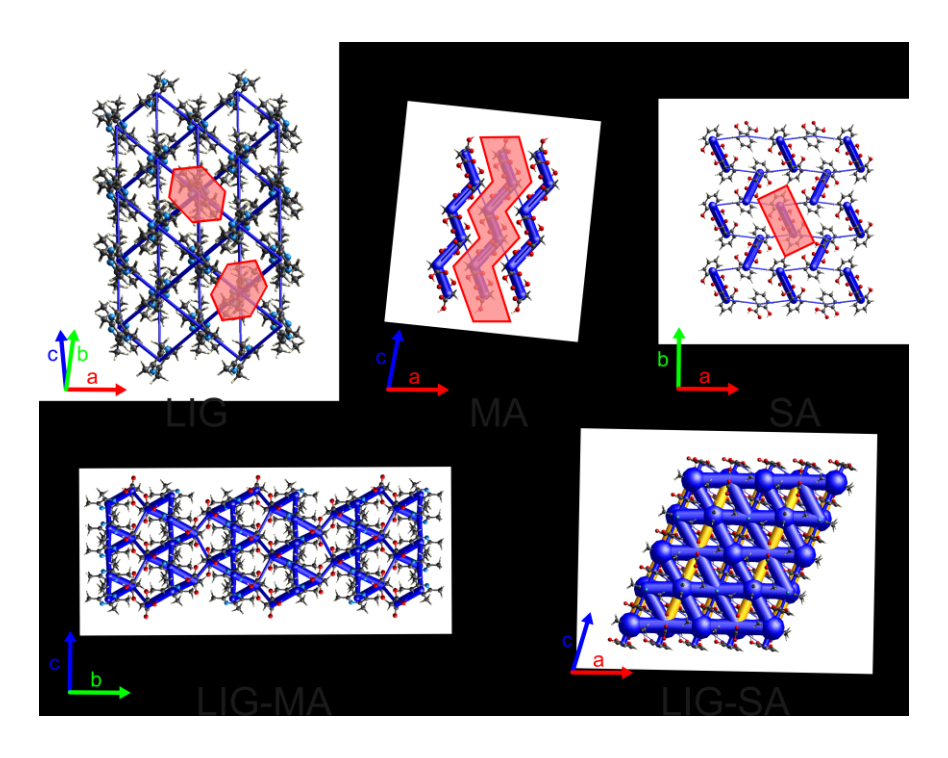


Figure 4. Energy framework analysis for the coformers and cocrystals.

MA has a zig-zag like interaction energy framework between MA molecules in the bc plane, where facile slip among parallel slip planes is only sterically unhindered in the  $[010]/[0\bar{1}0]$  direction. However, the intermolecular energy between layers is low (Figure 4). Consequently, it exhibits a reasonably high plasticity ( $P_{y,i} = 66.4 \text{ MPa}$ ), similar to SA. For LIG-MA, hydrogen-bonded columns exist, but the interaction energies between columns are high, resulting in a lower plasticity ( $P_{y,i} = 74.2 \text{ MPa}$ ) than LIG, SA, and MA. Despite this lower plasticity, LIG-MA has slightly improved tabletability compared to MA alone, and a higher tabletability than LIG at pressures >150 MPa due to a lack of overcompression (Figure 3a).

Overall, the plasticity of the five crystal forms in this work follows the descending order of LIG > MA  $\approx$  SA  $\geq$  LIG-MA > LIG-SA according to the  $P_{y,i}$  values (Table 1). This rank order can be qualitatively justified using an energy framework analysis of their crystal structures.

## 3.4 BA-BS interplay

To justify the observation of low plasticity, and thus low BA due to less extensive plastic deformation during compaction, yet high tabletability of LIG-SA, the interplay between BA and BS must be considered. A higher BS can compensate the detrimental effect on tabletability of a smaller BA between particles (Sun, 2009). This may be examined by comparing their compactibility plots (Figure 5a) and their  $\sigma_0$  values (Table 1), which can be used to quantify apparent bonding strength. The  $\sigma_0$  value of LIG-SA (5.72 MPa) is higher than SA (3.79 MPa) and LIG (1.98 MPa), confirming that the BS of LIG-SA is significantly higher than LIG and this positive effect outweighs the negative effect of deteriorated BA on tabletability due to the low plasticity of LIG-SA.

The  $\sigma_0$  value of LIG-MA (2.65 MPa) is also higher than MA (1.31 MPa) and LIG (1.98 MPa). However, the advantage of a higher BS of LIG-MA is not sufficient to compensate the negative effects of its lower BA on tabletability. Hence, the tabletability of LIG-MA is lower than LIG and only slightly higher than that of MA.

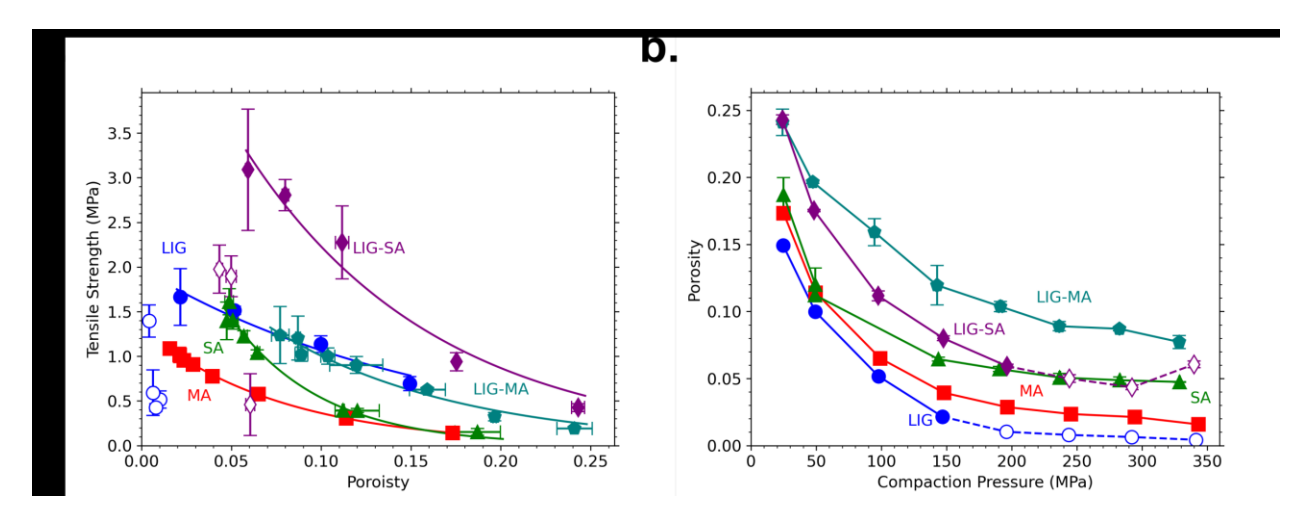


**Figure 5.** (a) Compactibility and (b) compressibility for LIG (blue circles), MA (red squared), SA (green triangles), LIG-MA (teal pentagons), and LIG-SA (purple diamonds). Open symbols indicate overcompressed tablets and were omitted from any fitting.

**Table 1.** Key material properties  $(\rho_t, \sigma_0, b, \text{ and } P_{y,i})$  for the five powders investigated in this work. Values in parentheses indicate the standard deviation from the last five measurements for  $\rho_t$ , the standard errors of fitting for  $\sigma_0$  and b, and the standard deviation of three separate measurements for  $P_{y,i}$ .

Material	$\rho_t  (\text{g/cm}^3)$	$\sigma_0$ (MPa)	b	$P_{y,i}$ (MPa)
LIG	1.0952 (0.0016)	1.98 (0.13)	6.2 (1.0)	52.5 (0.6)
MA	1.6158 (0.0002)	1.31 (0.03)	12.9 (0.6)	66.4 (0.3)
SA	1.4365 (0.0001)	3.79 (0.33)	19.6 (1.6)	68.3 (0.2)
LIG-MA	1.2666 (0.0004)	2.65 (0.33)	9.7 (1.2)	74.2 (0.1)
LIG-SA	1.3251 (0.0001)	5.72 (0.67)	9.4 (1.3)	90.1 (1.5)

This work not only highlights API tabletability modulation using cocrystallization but also underscores the broader significance of considering the BA and BS interplay when predicting tabletability. It is important to recognize that a crystal form with lower plasticity may still exhibit higher tabletability as the positive contribution of a higher BS may outcompete the negative effect of a smaller BA. Future studies could explore establishing criteria for attaining a higher overall tensile strength with crystals exhibiting different plasticity. Investigating the nuanced relationship between plasticity, BA, and BS will contribute to refining the guidelines for crystal engineering, enabling the design of pharmaceutical crystals with optimal mechanical properties.

## 4 Conclusion

The improved tabletability of LIG-SA compared to LIG suggests that the new LIG-SA salt cocrystal may be a promising crystal form for tableting. More importantly, this work affirms the potential of cocrystallization in modulating API mechanical properties and highlights the importance of considering the BA-BS interplay in studies of crystal tabletability. It exemplifies

that a less plastic crystal form may still exhibit a higher tabletability when the positive effect of a higher bonding strength outcompetes the negative effect of a smaller bonding area. This nuanced understanding is crucial for advancing crystal engineering strategies in pharmaceutical research.

294

## Acknowledgements

CCS thanks the National Science Foundation for support through the Industry University Collaborative Research Center grant IIP-2137264, Center for Integrated Materials Science and Engineering for Pharmaceutical Products (CIMSEPP).

## References

- Aprà, E., Bylaska, E.J., de Jong, W.A., Govind, N., Kowalski, K., Straatsma, T.P., Valiev, M., van Dam, H.J.J., Alexeev, Y., Anchell, J., Anisimov, V., Aquino, F.W., Atta-Fynn, R., Autschbach, J., Bauman, N.P., Becca, J.C., Bernholdt, D.E., Bhaskaran-Nair, K., Bogatko, S., Borowski, P., Boschen, J., Brabec, J., Bruner, A., Cauët, E., Chen, Y., Chuev, G.N., Cramer, C.J., Daily, J., Deegan, M.J.O., Dunning, T.H., Dupuis, M., Dyall, K.G., Fann, G.I., Fischer, S.A., Fonari, A., Früchtl, H., Gagliardi, L., Garza, J., Gawande, N., Ghosh, S., Glaesemann, K., Götz, A.W., Hammond, J., Helms, V., Hermes, E.D., Hirao, K., Hirata, S., Jacquelin, M., Jensen, L., Johnson, B.G., Jónsson, H., Kendall, R.A., Klemm, M., Kobayashi, R., Konkov, V., Krishnamoorthy, S., Krishnan, M., Lin, Z., Lins, R.D., Littlefield, R.J., Logsdail, A.J., Lopata, K., Ma, W., Marenich, A.V., Martin del Campo, J., Mejia-Rodriguez, D., Moore, J.E., Mullin, J.M., Nakajima, T., Nascimento, D.R., Nichols, J.A., Nichols, P.J., Nieplocha, J., Otero-de-la-Roza, A., Palmer, B., Panyala, A., Pirojsirikul, T., Peng, B., Peverati, R., Pittner, J., Pollack, L., Richard, R.M., Sadayappan, P., Schatz, G.C., Shelton, W.A., Silverstein, D.W., Smith, D.M.A., Soares, T.A., Song, D., Swart, M., Taylor, H.L., Thomas, G.S., Tipparaju, V., Truhlar, D.G., Tsemekhman, K., Van Voorhis, T., Vázquez-Mayagoitia, Á., Verma, P., Villa, O., Vishnu, A., Vogiatzis, K.D., Wang, D., Weare, J.H., Williamson, M.J., Windus, T.L., Woliński, K., Wong, A.T., Wu, Q., Yang, C., Yu, Q., Zacharias, M., Zhang, Z., Zhao, Y., Harrison, R.J., 2020. NWChem: Past, future. J. Chem. present, and Phys. 152, 184102. https://doi.org/10.1063/5.0004997
- Cao, S., Zhao, W., Bu, H., Zhao, Y., Yu, C., 2016. Ligustrazine for the treatment of unstable angina: A meta-analysis of 16 randomized controlled trials. eCAM 2016, e8617062. https://doi.org/10.1155/2016/8617062
- Chang, S.-Y., Wang, C., Sun, C.C., 2019. Relationship between hydrate stability and accuracy of true density measured by helium pycnometry. Int. J. Pharm. 567, 118444. https://doi.org/10.1016/j.ijpharm.2019.06.035

- Chattoraj, S., Shi, L., Sun, C.C., 2010. Understanding the relationship between crystal structure, plasticity and compaction behaviour of theophylline, methyl gallate, and their 1: 1 co-crystal. CrystEngComm 12, 2466–2472. https://doi.org/10.1039/C000614A
- Childs, S.L., Stahly, G.P., Park, A., 2007. The salt-cocrystal continuum: The influence of crystal structure on ionization state. Mol. Pharmaceutics 4, 323–338. https://doi.org/10.1021/mp0601345
- Chow, S.F., Chen, M., Shi, L., Chow, A.H.L., Sun, C.C., 2012. Simultaneously improving the mechanical properties, dissolution performance, and hygroscopicity of ibuprofen and flurbiprofen by cocrystallization with nicotinamide. Pharm Res 29, 1854–1865. https://doi.org/10.1007/s11095-012-0709-5
- Dolomanov, O.V., Bourhis, L.J., Gildea, R.J., Howard, J.A.K., Puschmann, H., 2009. it OLEX2: a complete structure solution, refinement and analysis program. J. Appl. Crystallogr. 42, 339–341. https://doi.org/10.1107/S0021889808042726
- Fell, J.T., Newton, J.M., 1970. Determination of tablet strength by the diametral-compression test. J. Pharm. Sci. 59, 688–691. https://doi.org/10.1002/jps.2600590523
- Gao, H., Liu, P., Li, P., Huang, Z., Yu, F., Lei, T., Chen, Y., Cheng, Y., Mu, Q., Huang, H., 2015. Ligustrazine monomer against cerebral ischemia-reperfusion injury. Neural Regen. Res. 10, 832. https://doi.org/10.4103/1673-5374.156991
- Guo, M., Liu, Y., Shi, D., 2016. Cardiovascular actions and therapeutic potential of tetramethylpyrazine (active component isolated from *Rhizoma Chuanxiong*): Roles and mechanisms. BioMed. Res. Int. 2016, 2430329. https://doi.org/10.1155/2016/2430329
- Heckel, R.W., 1961a. An analysis of powder compaction phenomena. Trans. Metall. Soc. AIME 221, 1001–1008.
- Heckel, R.W., 1961b. Density-pressure relationships in powder compaction. Trans. Metall. Soc. AIME 221, 671–675.
- Hu, S., Wang, C., He, X., Sun, C.C., 2020. Reducing the sublimation tendency of ligustrazine through salt formation. Cryst. Growth Des. 20, 2057–2063. https://doi.org/10.1021/acs.cgd.9b01704
- Kao, T.-K., Ou, Y.-C., Kuo, J.-S., Chen, W.-Y., Liao, S.-L., Wu, C.-W., Chen, C.-J., Ling, N.-N., Zhang, Y.-H., Peng, W.-H., 2006. Neuroprotection by tetramethylpyrazine against ischemic brain injury in rats. Neurochem. Int. 48, 166–176. https://doi.org/10.1016/j.neuint.2005.10.008
- Karki, S., Friščić, T., Fábián, L., Laity, P.R., Day, G.M., Jones, W., 2009. Improving mechanical properties of crystalline solids by cocrystal formation: new compressible forms of paracetamol. Adv. Mat. 21, 3905–3909. https://doi.org/10.1002/adma.200900533
- Kortüm, G., Vogel, W., Andrussow, K., 1960. Disssociation constants of organic acids in aqueous solution. Pure Appl. Chem. 1, 187–536. https://doi.org/10.1351/pac196001020187
- Kuentz, M., Leuenberger, H., 1999. Pressure susceptibility of polymer tablets as a critical property:

  A modified Heckel equation. J. Pharm. Sci. 88, 174–179. https://doi.org/10.1021/js980369a
- Li, L., Chu, L., Fang, Y., Yang, Y., Qu, T., Zhang, J., Yin, Y., Gu, J., 2017. Preconditioning of bone marrow-derived mesenchymal stromal cells by tetramethylpyrazine enhances cell migration and improves functional recovery after focal cerebral ischemia in rats. Stem Cell Res Ther 8, 112. https://doi.org/10.1186/s13287-017-0565-7

- Liao, S.-L., Kao, T.-K., Chen, W.-Y., Lin, Y.-S., Chen, S.-Y., Raung, S.-L., Wu, C.-W., Lu, H.-C., Chen, C.-J., 2004. Tetramethylpyrazine reduces ischemic brain injury in rats. Neuroscience Letters 372, 40–45. https://doi.org/10.1016/j.neulet.2004.09.013
- Lin, K.-H., Kuo, W.-W., Jiang, A.-Z., Pai, P., Lin, J.-Y., Chen, W.-K., Day, C.H., Shen, C.-Y., Padma, V.V., Huang, C.Y., 2015. Tetramethylpyrazine ameliorated hypoxia-induced myocardial cell Apoptosis via HIF-1α/JNK/p38 and IGFBP3/BNIP3 inhibition to upregulate PI3K/Akt survival signaling. Cell. Physiol. Biochem. 36, 334–344. https://doi.org/10.1159/000374076
- Liu, L., Wang, C., Dun, J., Chow, A.H.L., Sun, C.C., 2018. Lack of dependence of mechanical properties of baicalein cocrystals on those of the constituent components. CrystEngComm 20, 5486–5489. https://doi.org/10.1039/C8CE00787J
- Mackenzie, C.F., Spackman, P.R., Jayatilaka, D., Spackman, M.A., 2017. it CrystalExplorer model energies and energy frameworks: extension to metal coordination compounds, organic salts, solvates and open-shell systems. IUCrJ 4, 575–587. https://doi.org/10.1107/S205225251700848X
- O'Neil, M.J. (Ed.), 2006. The Merck index: An encyclopedia of chemicals, drugs, and biologicals, 14th ed. Merck Reasearch Laboratories, Whitehouse Station, N.J.
- Osei-Yeboah, F., Chang, S.-Y., Sun, C.C., 2016. A critical examination of the phenomenon of bonding area-bonding strength interplay in powder tableting. Pharm. Res. 33, 1126–1132.
- Paul, S., Chang, S.-Y., Sun, C.C., 2017. The phenomenon of tablet flashing its impact on tableting data analysis and a method to eliminate it. Powder Technol. 305, 117–124. https://doi.org/10.1016/j.powtec.2016.09.054
- Paul, S., Sun, C.C., 2017. Gaining insight into tablet capping tendency from compaction simulation. Int. J. Pharm. 524, 111–120. https://doi.org/10.1016/j.ijpharm.2017.03.073
- Ren, Z., Ma, J., Zhang, P., Luo, A., Zhang, S., Kong, L., Qian, C., 2012. The effect of ligustrazine on L-type calcium current, calcium transient and contractility in rabbit ventricular myocytes. J. Ethnopharmacol. 144, 555–561. https://doi.org/10.1016/j.jep.2012.09.037
- Ryshkewitch, E., 1953. Compression strength of porous sintered alumina and zirconia. J. Am. Ceram. 36, 65–68. https://doi.org/10.1111/j.1151-2916.1953.tb12837.x
- Sheldrick, G.M., 2015a. 1t SHELXT Integrated space-group and crystal-structure determination. Acta Crystallogr. A 71, 3–8. https://doi.org/10.1107/S2053273314026370
- Sheldrick, G.M., 2015b. Crystal structure refinement with it SHELXL. Acta Crystallogr. C 71, 3–8. https://doi.org/10.1107/S2053229614024218
- Spackman, P.R., Turner, M.J., McKinnon, J.J., Wolff, S.K., Grimwood, D.J., Jayatilaka, D., Spackman, M.A., 2021. It CrystalExplorer: a program for Hirshfeld surface analysis, visualization and quantitative analysis of molecular crystals. J. Appl. Crystallogr. 54, 1006–1011. https://doi.org/10.1107/S1600576721002910
- Sun, C.C., 2011. Decoding powder tabletability: Roles of particle adhesion and plasticity. J. Adhes. Sci. Technol. 25, 483–499. https://doi.org/10.1163/016942410X525678
- Sun, C.C., 2009. Materials science tetrahedron—A useful tool for pharmaceutical research and development. J. Pharm. Sci. 98, 1671–1687. https://doi.org/10.1002/jps.21552
- Sun, C.C., 2004. A novel method for deriving true density of pharmaceutical solids including hydrates and water-containing powders. J. Pharm. Sci. 93, 646–653. https://doi.org/10.1002/jps.10595
- Sun, C.C., Hou, H., 2008. Improving mechanical properties of caffeine and methyl gallate crystals by cocrystallization. Cryst. Growth Des. 8, 1575–1579. https://doi.org/10.1021/cg700843s

- Sun, C.C., Hou, H., Gao, P., Ma, C., Medina, C., Alvarez, F.J., Hou, H., Gao, P., 2009. Development of a high drug load tablet formulation based on assessment of powder manufacturability: Moving towards quality by design. J. Pharm. Sci. 98, 239–247. https://doi.org/10.1002/jps.21422
- Vreeman, G., Sun, C.C., 2022. Air entrapment during tablet compression Diagnosis, impact on tableting performance, and mitigation strategies. Int. J. Pharm. 615, 121514. https://doi.org/10.1016/j.ijpharm.2022.121514
- Vreeman, G., Sun, C.C., 2021. Mean yield pressure from the in-die heckel analysis is a reliable plasticity parameter. Int. J. Pharm. X 3, 100094. https://doi.org/10.1016/j.ijpx.2021.100094
- Vreeman, G., Wang, C., Reddy, C.M., Sun, C.C., 2021. Exceptional powder tabletability of elastically flexible crystals. Cryst. Growth Des. 21, 6655–6659. https://doi.org/10.1021/acs.cgd.1c01017
- Wang, C., Paul, S., Sun, D.J., Nilsson Lill, S.O., Sun, C.C., 2020. Mitigating punch sticking propensity of celecoxib by cocrystallization: an integrated computational and experimental approach. Cryst. Growth Des. 20, 4217–4223. https://doi.org/10.1021/acs.cgd.0c00492
- Xiang, T., Sun, C.C., 2023. Worsened punch sticking by external lubrication with magnesium stearate. Int. J. Pharm. 123636. https://doi.org/10.1016/j.ijpharm.2023.123636
- Zhao, Y., Liu, Y., Chen, K., 2016. Mechanisms and clinical application of tetramethylpyrazine (an interesting natural compound isolated from Ligusticum Wallichii): Current status and perspective. Oxid. Med. Cell. Longevity 2016, 2124638. https://doi.org/10.1155/2016/2124638
- Zheng, Q., Huang, Y., Zhu, P., Tong, Q., Bao, X., Zhang, Q., Zheng, G., Wang, Y., 2018. Ligustrazine exerts cardioprotection in animal models of myocardial ischemia/reperfusion injury: Preclinical evidence and possible mechanisms. Front. Pharmacol. 9. https://doi.org/10.3389/fphar.2018.00729